ChemComm

COMMUNICATION

View Article Online
View Journal





Cite this: DOI: 10.1039/c7cc02838e

Received 23rd March 2017,
Accepted 11th May 2017

DOI: 10.1039/c7cc02838e

rsc.li/chemcomm

# Novel Ag-doped glass frits for high-efficiency crystalline silicon solar cells†

Sheng Yuan, Yongji Chen, Zongwei Mei, Ming-Jian Zhang, Zhou Gao, Xingbo Wang, Xing Jiang and Feng Pan *

**Glass frits play an important role in the front contact electrodes of crystalline silicon (c-Si) solar cells. In this work, we developed a novel glass frit by doping Ag into a glass frit in the process of high-temperature synthesis. When the Ag paste including this novel glass frit was used as the front contact electrode of silicon solar cells, the conversion efficiency of poly-crystalline silicon (pc-Si) solar cells was improved by 1.9% compared to the glass frit without Ag. Through SEM characterisation and calculation of series resistance, we further found that the interface between Ag and Si was improved and the contact resistance of Ag and Si was greatly reduced, which were believed to be responsible for the improvement of solar cell performance. This work shows great guidance significance to develop novel and highly efficient commercial glass frits applied in solar cells in the future.**

As we know, crystalline silicon solar cells have occupied a major market share in the photovoltaic market due to their advantages of environment-friendly character and high power conversion efficiency (PCE).[1–5] Recently more and more researchers paid attention to developing low-cost and high-efficiency front contact electrodes of crystalline silicon solar cells;[6–11] Ag paste is the first choice to prepare the front contact electrodes. It consists of Ag powder, glass frit and organic carrier.[12,13] Among them, the content of glass frit is the least, but it is essential for solar cells to gain a good performance. In the fabrication of front contact electrodes, the glass frit will etch through passivation and anti-reflection coating ($SiN_x$ layer) in the sintering process of c-Si solar cells, which will form a good Ohmic contact between Ag and Si.[14–17]

During the sintering process, traditional glass frits will experience several changes with temperature increase. Firstly glass frits begin to soften and flow to the surface of the $SiN_x$ layer under the influence of gravity. Then etching reaction will take place on the surface (reaction (1) seen below).[18,19] With a further increase of the temperature, part of silver particles in Ag paste will be oxidized and dissolved into glass frits (reaction (3) seen below), which will further accelerate the etching process, because $Ag_2O$ can also etch the $SiN_x$ layer (reaction (2)).[14,16,20] Some neutral Ag atoms are produced through reaction (2). When temperature reduces, these Ag atoms will be recrystallized into Ag nanoparticles in the interfacial glass layer.[20–22] Our previous work showed that the concentration of these Ag nanoparticles had an important effect on the efficiency of c-Si solar cells.[21] A large concentration of Ag nanoparticles in the glass layer between Ag and the n-Si layer brings about a good Ohmic contact between the front contact electrodes and the n-Si layer. Conversely, a large contact resistance between Ag and the n-Si layer will be generated,[21–24] which was unfavorable for electron transfer from the n-Si layer to the contact electrodes. So we try to increase the concentration of Ag in the glass frit. It is hard for traditional glass frits to increase the concentration of Ag during the sintering process. Although some groups reported several methods for increasing the concentration of Ag in the glass frit such as increasing the sintering temperature,[14,25] increasing the amount of $O_2$ in the sintering atmosphere during the sintering process[26,27] and enhancing the content of PbO in the glass frit,[20,28] they all showed some disadvantages and the effect was not obvious.

$$2PbO + SiN_x \rightarrow 2Pb + SiO_2 + \frac{x}{2}N_2 \quad (1)$$

$$2Ag_2O + SiN_x \rightarrow 4Ag + SiO_2 + \frac{x}{2}N_2 \quad (2)$$

$$4Ag + O_2 \rightarrow 2Ag_2O \quad (3)$$

$$2Ag_2O + Si \rightarrow 4Ag + SiO_2 \quad (4)$$

According to the work of the Hest group,[14] we know that PbO in the glass frit began to etch the $SiN_x$ antireflective-coating at 500 °C (reaction (1)). Above 650 °C, Ag (from Ag particles in Ag paste) began to dissolve into the molten glass frit by reaction (3) and reacted with the $SiN_x$ layer (reaction (2)). If Ag is doped in

*School of Advanced Materials, Peking University Shenzhen Graduate School, Shenzhen, 518055, China. E-mail: panfeng@pkusz.edu.cn*

† Electronic supplementary information (ESI) available. See DOI: 10.1039/c7cc02838e

glass frits during the preparation of glass frits, $Ag^{+}$ doped in glass frits will be reduced to many neutral Ag atoms in the sintering process in advance, because the equilibrium reduction potential of $Ag^{+}$ is higher than that of $Pb^{2+}$ in glass frits.[16,26] As the temperature increases further, extra Ag (from Ag particles in Ag paste) is oxidized and dissolved in glass frits. Then they are reduced to Ag atoms in glass frits. When solar cells are cooled, more Ag atoms will be recrystallized into more dense Ag nanocrystals in the interfacial glass layer than that obtained by applying no Ag-doped glass frits.[16]

So we choose a novel way to implement our purpose by doping Ag ions into glass frits during the preparation of glass frits. We infer that the performance of solar cells will be improved using this kind of glass frit instead of a traditional one.

In this work, we successfully fabricated a Ag ion doped glass frit for the first time, and it was used to prepare Ag paste. The paste with the Ag ion doped (Ag-doped) glass frit was used as the front contact electrode. The following experimental results also confirmed our previous assumption. With an increase of Ag ion doping content in the glass frit, the performance of solar cells was enhanced. When 6 wt% Ag ions were doped, the conversion efficiency of polycrystalline silicon solar cells reached the highest value of 17.8% (improved 1.9% compared to traditional Pb–Te–O glass). The enhanced performance was ascribed to an excellent Ag/Si interface and low contact resistance. We found that the concentration of Ag nanoparticles remarkably increased in the interfacial glass layer compared to the glass frit without Ag ions. In addition, interestingly, we found that the Ag doped glass frit showed lower glass transition temperature ($T_g$) than the traditional Pb–Te–O glass frit, which indicates that the glass could soften faster and flow to the surface of the $SiN_x$ layer. We assume that it is helpful to uniformly etch the $SiN_x$ layer.

To fabricate uniform Ag-doped glass frits, we develop a facile and effective method. $AgNO_3$ with certain mass percentages (2%, 4%, 6%, 8% and 10%) was dissolved in deionized water. Next, other metal oxides (PbO, $TeO_2$ and $Bi_2O_3$) were subsequently added to the $AgNO_3$ solution and stirred to mix well with each other. Then the suspension was dried at 60 °C for 20 min. The obtained solid mixture was put in a furnace and heated at 1000 °C to melt. Then melt-mixed blends were water-quenched to room temperature by melt-quenching technology. Finally, through ball-milling, the fabrication of glass frits was fully completed. The obtained glass frits are shown in Fig. S1 (ESI†), and their color changes from white to grey and then to black with the increase of Ag doping content. Firstly, to determine the reaction product, X-ray diffraction (XRD) of Ag-doped glass was carried out. Fig. 1a shows the XRD patterns of six glass frits with different Ag doping content. All the XRD results of Ag-doped glass frits are similar to traditional Pb–Te–O glass (0% Ag-glass) in previous reports,[25,28] and they do not have obvious crystal peaks except for the board peak at 28.5°. According to these results, the amorphous nature of the six glass frits was confirmed. Furthermore, we did not find any peaks belonging to $Ag_2O$ or Ag crystals (Fig. S2, ESI†). This indicates that an amorphous Ag-doped glass frit was successfully synthesized.

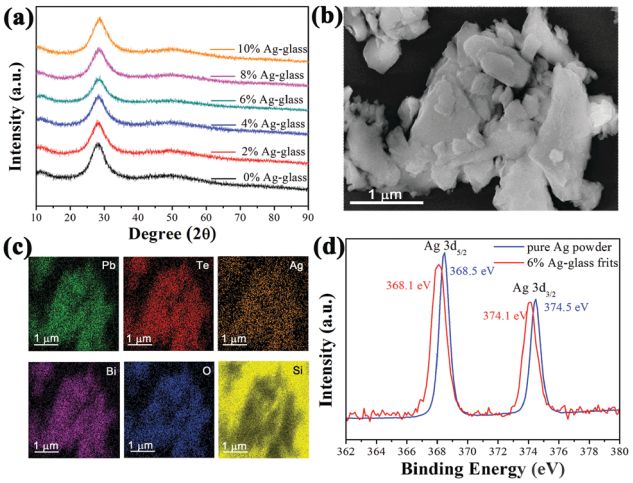


Fig. 1 (a) The XRD patterns of the Ag doped glass frit with different mass percentages of silver (0–10 wt%). (b) SEM image of the Ag (6 wt%) doped glass frit. (c) Corresponding elementary mapping of Pb, Te, Ag, Bi, O and Si. (d) The XPS spectra of Ag 3d for 6% Ag-glass powder and pure Ag powder.

In order to further ensure that Ag was fully and uniformly doped into a glass frit, we performed EDX analysis on the Ag-doped glass frit. Fig. 1b shows the SEM image of the obtained Ag-doped glass frit (6% Ag-glass). We can see that Ag-doped glass frit particles are irregular and the size of the Ag-doped glass frit particles is about 200 nm–2 μm. Fig. 1c shows the corresponding energy X-ray spectroscopy (EDX) elementary mapping images. It clearly displays that Pb, Te, Ag, Bi and O evenly distribute in the Ag-doped glass frit, which implies that Ag is evenly doped into the glass frit. Moreover, due to the low Ag doping content, the intensity of the Ag signal was weaker than that of other elements. Note that the sample was placed on a monocrystalline silicon wafer for measurement, so the areas without glass frits in the elementary mapping image were full of silicon signals as shown in Fig. 1c. The mass percentage of elemental content was gained based on EDX measurement (Fig. S3, ESI†). The calculated mass percentage of Ag is 5.7%, which agrees well with the expected result (6 wt%). This demonstrates that Ag was uniformly and fully doped into the glass frit.

To further study the state of Ag existing in the glass frit, XPS spectra were recorded on an Ag-doped glass frit (6% Ag-glass). As shown in Fig. 1d, the peak of Ag 3d is observed, which further confirms the existence of Ag. The binding energies of Ag $3d_{5/2}$ and $3d_{3/2}$ peaks are 368.1 and 374.1 eV, respectively, which are lower than the values (368.5 and 374.5 eV) of metallic silver. In addition, Ag 3d peaks broaden in comparison with those of metal Ag. These results are in good agreement with previously published XPS data for $Ag_2O$.[29,30] Ag 3d peaks of $Ag_2O$ shift to lower binding energies than those of metal Ag, which is in contrast to ordinary metal oxides. Based on the analysis above, it can be concluded that Ag ions homogeneously exist in the form of $Ag_2O$ in the glass network.

To investigate the effect of Ag ion doping on thermal properties of the glass frit, Differential Scanning Calorimetry (DSC) was performed under an air atmosphere as shown in Fig. 2a.

 

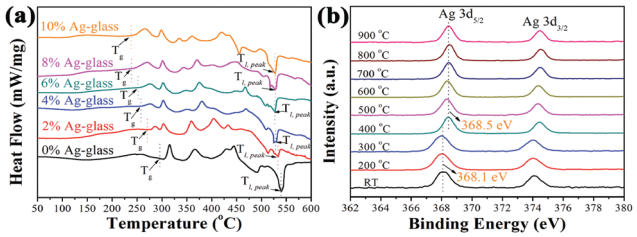


Fig. 2 (a) The DSC curves of the Ag-doped glass frit with different mass percentages of silver (0–10 wt%). (b) XPS spectra of Ag 3d for c-Si wafers with a $SiN_x$ layer coated with a thin 6% Ag-glass layer after annealing from 200 °C to 900 °C for 100 s, respectively.

Interestingly, we found that the glass transition temperature ($T_g$) and the liquefaction temperature ($T_{l,peak}$) of the Ag-doped glass frit were lower than those of the undoped glass frit. This means that Ag-doped glass will soften faster in the sintering process with a lower temperature (around $T$ = 250 °C), and flow to the $SiN_x$ layer for the etching reaction to take place compared to the undoped glass frit.

As a glass frit, its main function is to etch passivation and anti-reflection coating ($SiN_x$ layer). So, in order to study the etching procedure of Ag-doped glass, a simple experiment was designed. Some c-Si wafers with $SiN_x$ layers were coated with a thin 6%-Ag glass layer, and then these samples were annealed at different temperatures for 100 s in air, respectively. Next, XPS analysis of these samples was carried out as shown in Fig. 2b. With the increase of the annealing temperature, an obvious peak shift of Ag $3d_{3/2}$ from 368.1 eV to 368.5 eV is observed at 400 °C and the width of Ag 3d peaks becomes narrow at 400 °C. According to the previous description about XPS spectra of Ag 3d (Fig. 1d), these features of Ag 3d peaks should belong to Ag metal. This means that the etching reaction has already occurred at 400 °C (reaction (2)), which further confirms our previous inference. Moreover, according to the SEM and EDX characterization results of the sample after annealing at 400 °C for 100 s (Fig. S5, ESI†), occurrence of reaction (2) at 400 °C can also be determined.

In a typical fabrication procedure of the front contact electrodes, the as-synthesized glass frit was mixed with Ag powder for 20 min in a mortar, and then the organic phase was added to the mixture and mixed using a planetary mixer. Next, the paste was transferred to a three-roll grinder for further mixing and grinding. Finally the Ag paste was obtained. All semi-finished c-Si solar cells with $SiN_x$ layers and PN junctions were bought from a factory in Shenzhen. They were cut into the same size (4 cm × 5 cm) using a laser cutter. In order to strictly control the silver gridline parameters, gridlines were printed by a self-designed 3D printing machine.[21] Line spacing was 1.6 mm as shown in Fig. S6a (ESI†). The line width and height are 90 μm and 80 μm (Fig. S6c, ESI†), respectively. Then the c-Si solar cells with printed silver grids were dried in an oven and sintered in a furnace; the duration of sintering at 960 °C was about 10 s. Adopting six kinds of glass frits prepared above, we fabricated six corresponding cells. After the sintering procedure, the efficiency of c-Si solar cells was measured.

As shown in Fig. S6d (ESI†), $J$–$V$ characteristic curves are recorded for six solar cells to evaluate their performance.

Table 1 Performance comparison of solar cells with four different glass frits

| Sample | $J_{sc}$ (mA cm$^{-2}$) | $V_{oc}$ (V) | FF (%) | PCE (%) | $R_s$ (Ω cm$^2$) |
|---|---|---|---|---|---|
| 0% Ag-glass | 35.4 | 0.595 | 75.5 | 15.9 | 0.945 |
| 2% Ag-glass | 36.0 | 0.600 | 75.5 | 16.3 | 0.733 |
| 4% Ag-glass | 37.3 | 0.607 | 76.4 | 17.3 | 0.698 |
| 6% Ag-glass | 37.2 | 0.624 | 76.5 | 17.8 | 0.605 |
| 8% Ag-glass | 37.1 | 0.615 | 75.3 | 17.2 | 0.543 |
| 10% Ag-glass | 36.9 | 0.601 | 74.7 | 16.6 | 0.537 |

Series resistance was calculated through dark $J$–$V$ characteristic curves (inset in Fig. S6d, ESI†).[31] The details of their performance are shown in Table 1. A solar cell with a traditional glass frit was considered as the reference. Obviously, the performance of the cell (6% Ag-glass) was the best. In contrast to traditional glass frits, the efficiency of the cell was improved from 15.9% to 17.8%. Although pc-Si solar cells in our experiment are still traditional pc-Si solar cells without rear surface passivation and some novel light-trapping structures in the front n-Si layer, the highest efficiency of the cell with Ag-doped glass frits (17.8%) is much better than the efficiency of pc-Si solar cells (16.1–17.1%) with traditional structures reported in other literature reports.[32,33] Its series resistance was remarkably reduced. In addition, its short-circuit current density ($J_{sc}$), fill factor (FF) and open voltage ($V_{oc}$) were also further enhanced. This indicated that the Ag-doped glass frit is beneficial for optimization of efficiency. With a further increase of Ag ion doping content (8% and 10% Ag-glass), the series resistance was further reduced, but the performance of the solar cell gradually began to decrease. We speculated that although Ag ions doped in the glass frit can improve the Ag/Si interface,

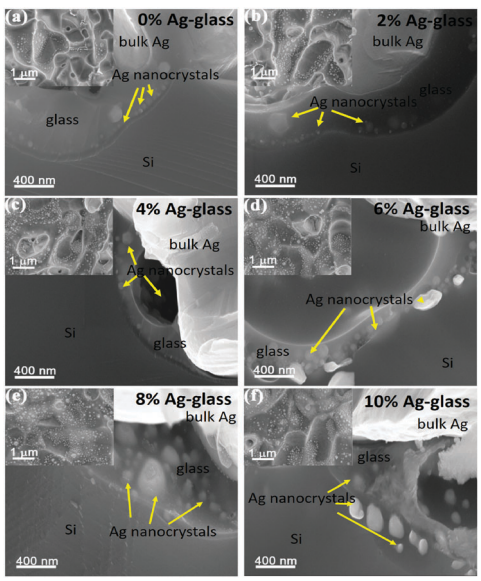


Fig. 3 The cross-sectional view of SEM micrographs of all solar cells: (a) 0% Ag-glass, (b) 2% Ag-glass, (c) 4% Ag-glass, (d) 6% Ag-glass, (e) 8% Ag-glass and (f) 10% Ag-glass; the insets display the plane view of SEM micrographs of the n-Si layer surface underneath Ag gridlines for the corresponding solar cell.

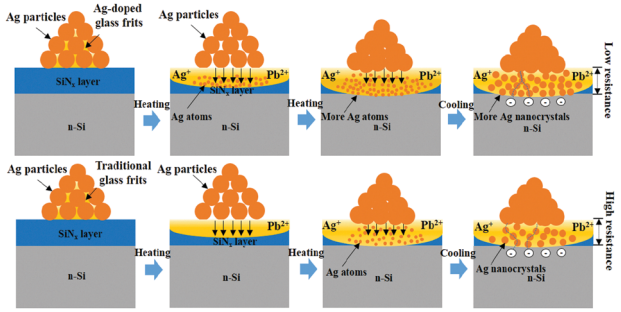


Fig. 4 The schematic diagram comparison of the formation of the front contact electrode using Ag-doped glass frits and traditional glass frits, respectively, during the sintering procedure.

excess Ag also enhanced the etching reaction which caused the n-Si layer of c-Si cells to destroy (reaction (4)).[14,25]

In order to prove our previous speculation about efficiency improvement, cross sections of all solar cells were characterized. As shown in Fig. 3, the Ag/Si interface could be clearly observed. We could easily identify Ag nanocrystals in the interfacial glass layer between n-Si and bulk Ag. Interestingly, we found that the concentration of Ag nanocrystals obviously increased with an increase of the Ag ion doping content, which was exactly agreeable with the previous assumption. In the meantime, to see more clearly the details of the interface, the bulk Ag was removed by immersing the cells in a 60% $HNO_3$ aqueous solution to only retain the interfacial glass layer on the n-Si layer. Thus, the plane graph of the glass layer was obtained (the top left inset in Fig. 3). A comparison of these planar SEM images also revealed that the c-Si solar cell with the Ag-doped glass frit formed more Ag crystals in the interfacial glass layer. These Ag nanocrystals could effectively improve the contact between bulk Ag and the Si layer. They were important bridges for the electrons to transfer and cross the interfacial glass layer. The above observations further explained why cells with Ag-doped glass have lower series resistance. In addition, we regarded that the lower glass transition temperature ($T_g$) also has a certain contribution to the improvement of performance. This can soften and reach the $SiN_x$ surface earlier, which will make etching more uniform and complete. A schematic diagram is shown in Fig. 4, which clearly illustrated the formation of the front contact electrode using Ag-doped glass frits and traditional glass frits, respectively, during the sintering procedure.

In summary, a novel Ag-doped glass frit was successfully fabricated for the first time. Ag ions were uniformly doped in the glass frit in the form of $Ag_2O$. Moreover, we found that Ag-doped glass has a lower glass transition temperature and liquefaction temperature than traditional glass, which may be advantageous to gain a good performance during the sintering process of c-Si solar cells and could reduce energy consumption. When it was applied in the front contact electrode of c-Si solar cells, a good efficiency was obtained, which was 1.9% higher than that of the solar cell adopting the traditional glass frit. It was ascribed to more dense Ag nanocrystals in the interfacial glass layer, which promoted the formation of good electrical contact between Ag and the n-Si layer and reduced the front contact resistance of solar cells. This work may open a new door for developing novel glass frits for c-Si solar cells.

We thank financial support from the Guangdong Innovative and Intrepreneurial Research Team Program (Grant No. 2013N080), the Peacock Plan (Grant No. KYPT20141016105435850), and the Shenzhen Key Lab (Grant No. (2012)780 and ZDSY20130331145131323).

## Notes and references

1 M. A. Green and S. P. Bremner, *Nat. Mater.*, 2016, **16**, 23.
2 K. Q. Peng and S. T. Lee, *Adv. Mater.*, 2011, **23**, 198.
3 A. Shah, P. Torres, R. Tscharner, N. Wyrsh and H. Keppner, *Science*, 1999, **285**, 692.
4 M. A. Green, *Prog. Photovoltaics*, 2009, **17**, 183–189.
5 A. Goeteberger, C. Hebling and H.-W. Schock, *Mater. Sci. Eng., R*, 2003, **40**, 1.
6 A. Dabirian, A. Lachowicz, J. W. Schüttauf, B. Paviet-Salomon, M. Morales-Masis, A. Hessler-Wyser, M. Despeisse and C. Ballif, *Sol. Energy Mater. Sol. Cells*, 2017, **159**, 243.
7 J. Jiang, Y. He, Z. Zhang, J. Wei and L. Li, *J. Alloys Compd.*, 2016, **689**, 662.
8 J.-D. Lee, H.-Y. Kwon, M.-J. Kim, E.-J. Lee, H.-S. Lee and S.-H. Lee, *Renewable Energy*, 2012, **42**, 1.
9 W.-H. Lee, T.-K. Lee and C.-Y. Lo, *J. Alloys Compd.*, 2016, **686**, 339.
10 X.-X. Pi, X.-H. Cao, J.-S. Chen, L. Zhang, Z.-X. Fu, L.-X. Wang and Q.-T. Zhang, *Rare Met.*, 2014, DOI: 10.1007/s12598-014-0301-8.
11 F. Tsin, J. Rousset, A. Le Bris and D. Lincot, *Prog. Photovoltaics*, 2016, **24**, 1123.
12 S. Thibert, J. Jourdan, B. Bechevet, S. Mialon, D. Chaussy, N. Reverdy-Bruas and D. Beneventi, *Prog. Photovoltaics*, 2016, **24**, 240.
13 B. Huang, W. Gan, G. Guo, Y. Li, T. Lin and X. Liu, *Ceram. Int.*, 2014, **40**, 393.
14 J. D. Fields, M. I. Ahmad, V. L. Pool, J. Yu, D. G. Van Campen, P. A. Parilla, M. F. Toney and M. F. van Hest, *Nat. Commun.*, 2016, **7**, 11143.
15 R. Hoenig, M. Duerrschnabel, W. van Mierlo, Z. Aabdin, J. Bernhard, J. Biskupek, O. Eibl, U. Kaiser, J. Wilde, F. Clement and D. Biro, *Energy Proc.*, 2013, **43**, 27.
16 H.-S. Kim, S.-B. Cho, H. Kim, D. Kim, M. Dovrat, G. Eytan and J.-Y. Huh, *Prog. Photovoltaics*, 2016, **24**, 1237.
17 G. Schubert, F. Huster and P. Fath, *Sol. Energy Mater. Sol. Cells*, 2006, **90**, 3399.
18 D.-Y. Shin, J.-Y. Seo, H. Tak and D. Byun, *Sol. Energy Mater. Sol. Cells*, 2015, **136**, 148.
19 Y. Tai, G. Zheng, H. Wang, H. Wang and J. Bai, *RSC Adv.*, 2015, **5**, 92515.
20 K.-K. Hong, S.-B. Cho, J. S. You, J.-W. Jeong, S.-M. Bea and J.-Y. Huh, *Sol. Energy Mater. Sol. Cells*, 2009, **93**, 898.
21 Y. Jiang, Y. Chen, M. Zhang, Y. Qiu, Y. Lin and F. Pan, *RSC Adv.*, 2016, **6**, 51871.
22 P. Kumar, M. Pfeffer, B. Willsch and O. Eibl, *Sol. Energy Mater. Sol. Cells*, 2016, **145**, 358.
23 P. Kumar, M. Pfeffer, B. Willsch, O. Eibl, L. J. Koduvelikulathu, V. D. Mihailetchi and R. Kopecek, *Sol. Energy Mater. Sol. Cells*, 2016, **157**, 200.
24 E. Cabrera, S. Olibet, J. Glatz-Reichenbach, R. Kopecek, D. Reinke and G. Schubert, *J. Appl. Phys.*, 2011, **110**, 114511.
25 J. Qin, W. Zhang, S. Bai and Z. Liu, *Appl. Surf. Sci.*, 2016, **376**, 52.
26 B.-M. Chung, S.-B. Cho, J.-W. Chun, Y.-S. Kim, K. Okamoto and J.-Y. Huh, *Electrochim. Acta*, 2013, **106**, 333.
27 J.-Y. Huh, K.-K. Hong, S.-B. Cho, S.-K. Park, B.-C. Lee and K. Okamoto, *Mater. Chem. Phys.*, 2011, **131**, 113.
28 J. Qin, W. Zhang, S. Bai and Z. Liu, *Sol. Energy Mater. Sol. Cells*, 2016, **144**, 256.
29 L. Yuan, L. Jiang, J. Liu, Z. Xia, S. Wang and G. Sun, *Electrochim. Acta*, 2014, **135**, 168.
30 K. T. Sullivan, C. Wu, N. W. Piekiel, K. Gaskell and M. R. Zachariah, *Combust. Flame*, 2013, **160**, 438.
31 D. Pysch, A. Mette and S. W. Glunz, *Sol. Energy Mater. Sol. Cells*, 2007, **91**, 1698.
32 J. Yoo, G. Yu and J. Yi, *Sol. Energy Mater. Sol. Cells*, 2011, **95**, 2.
33 X. Ye, S. Zou, K. Chen, J. Li, J. Huang, F. Cao, X. Wang, L. Zhang, X.-F. Wang, M. Shen and X. Su, *Adv. Funct. Mater.*, 2014, **24**, 6708.

 